Molecular Vision 2007; 13:545-48 <http://www.molvis.org/molvis/v13/a58/>
Received 9 November 2006 | Accepted 23 March 2007 | Published 4 April 2007

HTRA1 promoter polymorphism predisposes Japanese to age-related macular degeneration

Tsunehiko Yoshida,[1] Andrew DeWan,[2] Hong Zhang,[2] Ryosuke Sakamoto,[1] Haru Okamoto,[1] Masayoshi Minami,[1] Minoru Obazawa,[1] Atsushi Mizota,[3] Minoru Tanaka,[3] Yoshihiro Saito,[4] Ikue Takagi,[5] Josephine Hoh,[2] Takeshi Iwata[1]

(The first four authors contributed equally to this publication)

[1]National Institute of Sensory Organs, National Hospital Organization Tokyo Medical Center, Tokyo, Japan; [2]Department of Epidemiology and Public Health, Yale University School of Medicine, 60 College Street, New Haven CT 06520, [3]Department of Ophthalmology, Juntendo University Urayasu Hospital, Chiba, [4]Division of Ophthalmology, National Hospital Organization Osaka Medical Center, Osaka, [5]Division of Ophthalmology, National Hospital Organization Kyushu Medical Center, Fukuoka, Japan

Purpose: To study the effect of candidate single nucleotide polymorphisms (SNPs) on chromosome 10q26, recently shown to be associated with wet age-related macular degeneration (AMD) in Chinese and Caucasian cohorts, in a Japanese cohort.

Methods: Using genomic DNA isolated from peripheral blood of wet AMD cases and age-matched controls, we genotyped two SNPs, rs10490924, and rs11200638, on chromosome 10q26, 6.6 kb and 512 bp upstream of the *HTRA1* gene, respectively, using temperature gradient capillary electrophoresis (TGCE) and direct sequencing. Association tests were performed for individual SNPs and jointly with SNP complement factor H (CFH) Y402H.

Results: The two SNPs, rs10490924 and rs11200638, are in complete linkage disequilibrium (D'=1). Previous sequence comparisons among seventeen species revealed that the genomic region containing rs11200638 was highly conserved while the region surrounding rs10490924 was not. The allelic association test for rs11200638 yielded a p-value $<10^{-11}$. SNP rs11200638 conferred disease risk in an autosomal recessive fashion: Odds ratio was 10.1 (95% CI 4.36, 23.06), adjusted for SNP CFH 402, for those carrying two copies of the risk allele, whereas indistinguishable from unity if carrying only one risk allele.

Conclusions: The *HTRA1* promoter polymorphism, rs11200638, is a strong candidate with a functional consequence that predisposes Japanese to develop neovascular AMD.

Japanese patients are predominantly affected with vascular or "wet" AMD with little or no drusen deposition, in contrast to the Caucasian population which has a higher prevalence of drusen formation and the dry form of the disease. Association between the complement factor H (CFH) Y402H polymorphism (CFH 402) and age-related macular degeneration (AMD) has been shown in twelve or so different Caucasian populations [1,2]. However, that association failed to be replicated in Japanese populations, in which no control individual was found to be homozygous for the risk allele [3,4].

HTRA1 is a member of the heat shock serine proteases and is up-regulated by cellular stress. *HTRA1* is expressed in both the human and mouse retina [5,6]. Recently a promoter single nucleotide polymorphism (SNP) rs11200638 in *HTRA1* was shown to be highly associated with wet AMD [6,7]. Furthermore, *HTRA1* resides in a region of chromosome 10q26 that has been implicated as the "top" candidate region for AMD. Here we test two SNPs, rs10490924 (6.6 kb upstream of *HTRA1*), and rs11200638, for their association to wet AMD in a Japanese population.

Correspondence to: Josephine Hoh, Department of Epidemiology and Public Health, Yale University, 60 College Street, Room 416, New Haven CT 06520, Phone: (203) 785-6831; FAX: (203) 785-6279; email: josephine.hoh@yale.edu

METHODS

We genotyped 88 neovascular AMD cases and 97 AMD-free age-matched controls for SNPs rs10490924 and rs11200638. Case and control individuals were the same as our previous CFH association study [3] with all cases being characterized as AMD grade 5B [1]. Among cases the mean age was 74.8 years (standard deviation: s.d. 8.8 years) and 70.5% male; among controls the mean age was 71.1 years (s.d. 9.1 years), and 38.1% male. Informed consent was obtained from all participants, and the procedures used conformed to the tenets of the Declaration of Helsinki. Genotyping was performed as described previously [3]. Briefly, PCR was performed using primers designed to amplify the genomic region containing each SNP (rs10490924 forward: 5'-GGT GGT TCC TGT GTC CTT CA-3', reverse: 5'-GGG GTA AGG CCT GAT CAT CT-3'; rs11200638 forward: 5'-CGG ATG CAC CAA AGA TTC TCC-3', reverse: 5'-TTC GCG TCC TTC AAA CTA ATG G-3'). Following amplification, genotype determination was performed on the PCR products using either temperature gradient capillary electrophoresis (TGCE; Reveal SpectruMedix,

State College, PA) or through direct sequencing using CEQ2000XL DNA analysis system (Beckman Coulter, Fullerton, CA).

Hardy Weinberg equilibrium (HWE) χ^2 values in the entire sample and controls only were calculated to identify possible genotyping errors. No extreme deviations (χ^2>50) were observed (Table 1). Linkage disequilibrium (LD) was measured by the D' value. For each SNP, Pearson's χ^2 tests with one degree of freedom for association were performed. Odds ratios (OR), population attributable risks (PAR), and their respective confidence intervals were calculated, formula in [8].

Previous functional data lead us to focus further analyses on rs11200638 [6,7]. Joint ORs for two SNPs (rs11200638 and CFH 402, previously genotyped) were calculated using standard methods [9]. Marginal ORs and their confidence intervals for the two SNP were calculated using logistic regression with SNP CFH 402 and rs11200638 as independent variables [9]. PARs were calculated using standard methods [9]. Confidence intervals around the PARs were constructed using 999 bootstrap replicates. To control for confounding, the Mantel-Hanzel test for association with two variables was used [9]. Four genotypic models were considered (Full, Recessive, Multiplicative, and Dominant) and the Aikake information criterion (AIC) was utilized to assess the fit of each model. All R scripts used in the analysis are available upon request.

RESULTS

SNP rs11200638, approximately 6.1 kb downstream of the surrogate SNP rs10490924, resides in the promoter of the *HTRA1* serine protease gene (512 base pairs upstream of transcriptional start site). These two SNPs were in almost complete linkage disequilibrium (LD) and showed strong association with AMD in the Hong Kong study [6] and in a Caucasian population from Utah [7].

In our cohort, the two SNPs were also in complete LD, from which only two major (frequency >5%) haplotypes, one predominant in cases and one in controls, were observed. Disease association tests yielded p-values of 4.74×10^{-11} and 1.79×10^{-12} for rs10490924 and rs11200638, respectively (Table 1). Given the previous evidence of higher conservation across species [6] and the functional consequence of rs11200638 on *HTRA1* expression [6,7], additional analyses focused on this SNP.

Reanalyzing the original CFH genotype data, we found the OR covered unity (Table 2) and all interval estimates of PAR for CFH 402 variants under the four genotypic models included zero (Table 3). Of the four models, the best fit to the *HTRA1* SNP genotypic effects, as assessed by Akaike's information criterion, was the recessive model, from which the risk genotype was AA and non-risk was GG and GA (Table 3). Under the framework of recessive rs11200638 and the two observed genotypes for CFH 402, no interaction was detected between the two SNPs based on the likelihood ratio test (Table 3). Odds ratios for different genotypes of rs11200638 do not vary a great deal depending on the CFH 402 genotypes, and vice versa (Table 2). In fact, the OR curves shown in Figure 1 indicate a "removable" interaction between the two SNPs, in which the original two OR curves become parallel (i.e. no

Table 1. Association of chromosome 10q26 single nucleotide polymorphisms with age-related macular degeneration

Attribute	rs10490924 (G/T)	rs11200638 (G/A)
HWE χ^2-combined	5.4	7.6
-controls only	0.98	0.88
Risk allele	T	A
Frequency in case	0.68	0.69
Frequency in control	0.33	0.32
Allelic association χ^2 nominal p-value	4.74E-11	1.79E-12

To examine genotyping errors, Hardy Weinberg Equilibrium (HWE) χ^2 values are computed with cases and controls combined and controls alone. The age range is 51 to 90 years old with mean 74.8 and standard deviation (s.d.) 8.81 in cases, and 50 to 88 years old with mean 71.1 and s.d. 9.08 in controls.

Table 2. Odds ratios for the joint and marginal effects of single nucleotide polymorphisms complement factor H 402 and rs11200638 on age-related macular degeneration

	rs11200638		
CFH 402	GG/GA	AA	CFH 402 risk (adjusted for rs11200638)
TT	1	7.92	1
CT	1.11	30.52	1.41 (95% CI: 0.54,3.74)
rs11200638 risk adjusted for CFH	1	10.02; 95% CI: 4.36,23.06	

CFH indicates complement factor H. Joint odds ratios were calculated from standard formulae. Marginal odds ratios and 95% confidence intervals were calculated using logistic regression (see Methods) with each SNP was adjusted for the other.

interaction after transformation with a logarithmic function). Overall, after adjusting for the CFH 402 SNP, individuals carrying the risk homozygote AA of rs11200638 are greater than 10 times more likely to have AMD than those with the other genotypes (Table 2).

DISCUSSION

These data reconfirm the association of the *HTRA1* promoter SNP rs11200638, independent of the CFH 402 polymorphism, with wet AMD. The present study genotyped two previously identified disease associated SNPs in the chromosome 10q26 region. Both SNPs showed similar significance levels. The first SNP, rs10490924, resides in the hypothetical locus, LOC387715. Several studies have found significant association between AMD and this SNP [10-12]. So far only one transcript from this hypothetical locus has been identified in one experiment. No study has identified the transcript or protein in the retina, much less identified a change in the protein as a result of the SNP. Additionally, sequence comparisons of seventeen species presented in DeWan et al. show higher sequence

Table 3. Two-way analyses of complement factor H 402 and rs11200638

	PAR%		(95% CI)		M-H test: p-value	
Model for rs11200638	CFH 402	rs11200638	CFH 402	rs11200638	LRT p-value	AIC value
Full	3.4 (0, 9.7)	58.3 (50.5, 64.1)	0.07	8.30E-08	0.03	221.8
Recessive	4.6 (0, 10.7)	44 (40.5, 54.0)	0.23	6.20E-09	0.12	221.5
Multiplicative	1.7 (0, 7.8)	79.8 (73.0, 88.1)	*	*	0.02	225.7
Dominant	2.2 (0, 13.7)	58.6 (43.9, 78.9)	0.91	5.80E-04	0.1	246.9

Four genotypic models for rs11200638 are considered: Let r0, r1, and r2 be the marginal relative risks for genotypes GG, GA, and AA. Then, recessive model implies r0=r1; multiplicative model implies r1=r0r2; dominant model implies r2=r1; full model does not have any restriction on relative risks except that r0, r1, r2>0. The 95% confidence intervals (CI) of population attributable risk (PAR) were obtained via a bootstrap re-sampling method with 999 replicates. Mantel-Hanzel (M-H) tests are conducted for one SNP association adjusted for the other SNP; likelihood ratio tests (LRT) for joint single nucleotide polymorphism (SNP) association under a two-way multiplicative model: the relative risk (or OR) for any genotype pair (A, B) relative to the baseline pair (A0, B0) is the product of relative risk (or OR) of A relative to A0 and that of B relative to B0. AIC denotes the Akaike's information criterion to access goodness-of-fit for the rs11200638 model.

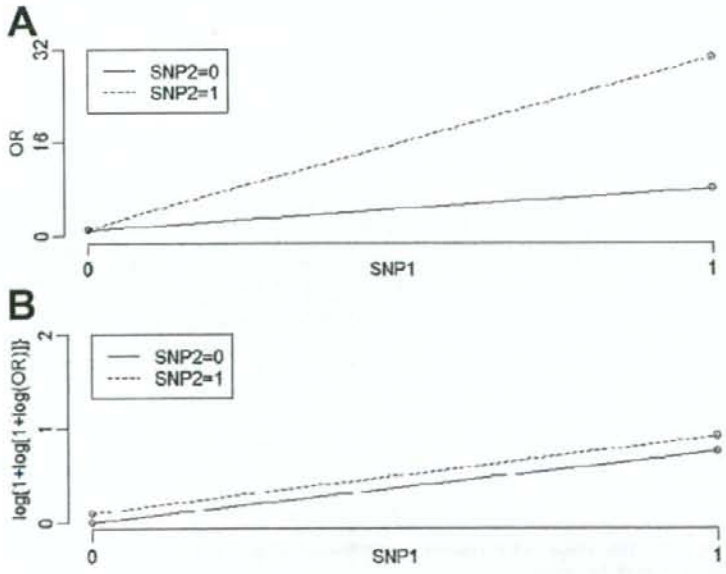

Figure 1. Odds ratio plots for two single nucleotide polymorphisms. Joint odds ratio plots for the single nucleotide polymorphisms (SNPs), complement factor H (CFH) 402, and rs11200638 before and after log transformation showing that the apparent interaction is a "removable" effect. SNP1=CFH 402: 0 is for TT and 1 is for CT; SNP2=rs11200638: 0 is for GG/GA and 1 is for AA. **A**: Original odds ratio (OR) curves: Height difference on the left is 1.11-1=0.11; height difference on the right is 30.52-7.92=22.60; slope for SNP2=0 is 7.92-1=6.92; slope for SNP2=1 is 30.52-1.11=29.41. **B**: Log(1+log(1+log)) transformation of the original OR.

conservation surrounding rs11200638 compared to that around rs10490924 [6]. *HTRA1* is expressed in the retina in humans [5] and mouse [6]. Computational analysis of the *HTRA1* promoter indicate that this SNP resides in a CpG island and may result in a change in the binding site for transcription factors AP2 and SRF [6]. Preliminary functional data suggest that individuals homozygous for the risk-allele at rs11200638 exhibit increased expression of *HTRA1* [6,7]. Therefore, given the existing functional data, it appears as if the *HTRA1* promoter polymorphism, rs11200638, is likely the underlying functional polymorphism in the 10q26 region. However, the mechanism to neovascularization is yet to be understood and will require intense investigation to uncover its link to the wet form of AMD.

ACKNOWLEDGEMENTS

This work was supported in part by grants from the National Institutes of Health and by awards from the Macular Vision Research Foundation and the Ellison Medical Foundation.

REFERENCES

1. Haddad S, Chen CA, Santangelo SL, Seddon JM. The genetics of age-related macular degeneration: a review of progress to date. Surv Ophthalmol 2006; 51:316-63.
2. Thakkinstian A, Han P, McEvoy M, Smith W, Hoh J, Magnusson K, Zhang K, Attia J. Systematic review and meta-analysis of the association between complement factor H Y402H polymorphisms and age-related macular degeneration. Hum Mol Genet 2006; 15:2784-90.
3. Okamoto H, Umeda S, Obazawa M, Minami M, Noda T, Mizota A, Honda M, Tanaka M, Koyama R, Takagi I, Sakamoto Y, Saito Y, Miyake Y, Iwata T. Complement factor H polymorphisms in Japanese population with age-related macular degeneration. Mol Vis 2006; 12:156-8.
4. Gotoh N, Yamada R, Hiratani H, Renault V, Kuroiwa S, Monet M, Toyoda S, Chida S, Mandai M, Otani A, Yoshimura N, Matsuda F. No association between complement factor H gene polymorphism and exudative age-related macular degeneration in Japanese. Hum Genet 2006; 120:139-43.
5. Tocharus J, Tsuchiya A, Kajikawa M, Ueta Y, Oka C, Kawaichi M. Developmentally regulated expression of mouse HtrA3 and its role as an inhibitor of TGF-beta signaling. Dev Growth Differ 2004; 46:257-74.
6. Dewan A, Liu M, Hartman S, Zhang SS, Liu DT, Zhao C, Tam PO, Chan WM, Lam DS, Snyder M, Barnstable C, Pang CP, Hoh J. HTRA1 promoter polymorphism in wet age-related macular degeneration. Science 2006; 314:989-92.
7. Yang Z, Camp NJ, Sun H, Tong Z, Gibbs D, Cameron DJ, Chen H, Zhao Y, Pearson E, Li X, Chien J, Dewan A, Harmon J, Bernstein PS, Shridhar V, Zabriskie NA, Hoh J, Howes K, Zhang K. A variant of the HTRA1 gene increases susceptibility to age-related macular degeneration. Science 2006; 314:992-3.
8. Armitage P. Statistical methods in medical research. New York: Wiley; 1971.
9. Scheffe, H. The Analysis of Variance. Wiley & Sons, New York, 1964.
10. Schmidt S, Hauser MA, Scott WK, Postel EA, Agarwal A, Gallins P, Wong F, Chen YS, Spencer K, Schnetz-Boutaud N, Haines JL, Pericak-Vance MA. Cigarette smoking strongly modifies the association of LOC387715 and age-related macular degeneration. Am J Hum Genet 2006; 78:852-64.
11. Rivera A, Fisher SA, Fritsche LG, Keilhauer CN, Lichtner P, Meitinger T, Weber BH. Hypothetical LOC387715 is a second major susceptibility gene for age-related macular degeneration, contributing independently of complement factor H to disease risk. Hum Mol Genet 2005; 14:3227-36.
12. Jakobsdottir J, Conley YP, Weeks DE, Mah TS, Ferrell RE, Gorin MB. Susceptibility genes for age-related maculopathy on chromosome 10q26. Am J Hum Genet 2005; 77:389-407.

The print version of this article was created on 4 Apr 2007. This reflects all typographical corrections and errata to the article through that date. Details of any changes may be found in the online version of the article.

85. 緑内障の動物モデル (1)
—霊長類モデル，ラットモデル—

岩田　岳
独立行政法人国立病院機構東京医療センター
臨床研究センター（感覚器センター）
分子細胞生物学研究部門

緑内障研究において動物モデルの存在はきわめて重要である．現在はおもに霊長類に加えてラットやマウスなどの齧歯（げっし）類が利用されている．本セミナーでは緑内障で利用されている動物モデルについて，2回シリーズで紹介したい．

はじめに

動物モデルの利点は，隅角や視神経・網膜における変化を発症過程に沿って詳細に解析できること，さらに新薬の評価を行えることである．これまでにも複数の哺乳類やその他の種で動物モデルの探索や開発が行われてきた[1]．利用目的に応じて1)ヒトとの視覚形態の類似性，2)発症までの時間，3)遺伝子操作の可能性，4)モデル動物作製に必要な技術，5)眼球の大きさ，6)解析に必要な技術，7)モデル動物の有効性，8)動物の維持費用などの検討が必要である．これまでにも異なる種で自然発症した緑内障モデル動物が紹介されているが，一般的には手術的あるいは遺伝子改変によって作製されたモデル動物が利用されている．

●霊長類モデル

すべての動物モデルのなかで隅角や視神経乳頭の構造がヒトと最も類似する霊長類モデルが研究に適していることはいうまでもないことである．特に房水流出機構に関する研究においては貴重な存在である．しかし，1頭当たりの維持費用がマウスの約100倍かかることや，飼育・管理に高度な知識・技術が必要であることから，多くの研究では利用されていない．房水流路の遮断にはおもに線維柱帯の光凝固が利用される[2,3]．この手法によって手術後数日間で25～60 mmHgの眼圧上昇が期待できる．その他の手法としては前房内に赤血球[4]，ラテックス[5]，ポリアクリルアミドゲル[6]，ステロイド[7]を注入することによって眼圧上昇を促す方法が報告されているが，光凝固によって最も安定した眼圧上昇が得られている[8]．霊長類における眼圧上昇は視神経乳頭，網膜神経線維，網膜神経節細胞層に障害[9]をもたらし，ヒトと同様な病理学的所見が再現されることが確認されている．また，霊長類モデルを利用した，光凝固後30日における網膜内の遺伝子発現の研究も報告されており[10]，この情報は新しい治療薬の開発にも利用されている．

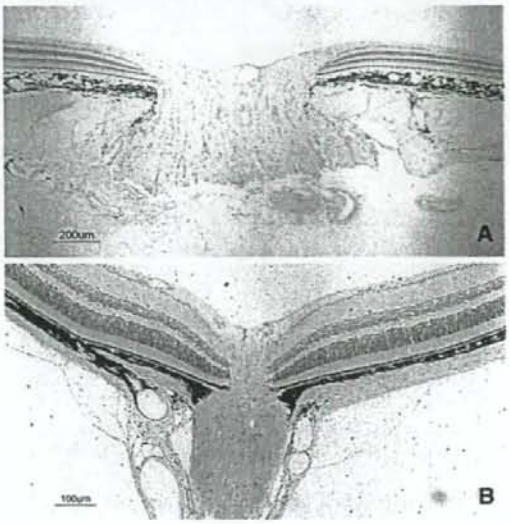

図1　カニクイザルとマウスの視神経乳頭の比較
カニクイザル（A）の視神経乳頭の構造はヒトときわめて類似しており，マウス（B）のそれとは大きく異なる．

●ラットモデル

動物モデルを用いて薬効評価を行う場合，実験には多数の動物が必要になる．このような場合にラットは有効である．ラットは簡単に飼育でき，性質もおとなしく，眼球も手ごろな大きさであることから，市販の機器を使って麻酔なしで眼圧測定ができる[11]．ラットの眼球には緑内障に関係する部位がすべて存在する．ラットにおける眼圧上昇は強膜静脈への生理食塩水の注入[12]，インドインクを使った線維柱帯の光凝固[13]，線維柱帯の光凝

0910-1810/07/¥100/頁/JCLS

固[14]，強膜静脈の焼灼[15]などの方法が用いられるが，研究者には高い技術が求められる．この方法によって最大約2倍眼圧上昇を急激に起こすことができる．眼圧上昇は通常数週間持続し，さらに2回目の光凝固が行われると，3週間以上の持続も可能である．眼圧上昇によってヒトに類似する網膜神経線維の萎縮や視神経乳頭の変化が観察できる[16,17]．ラットモデルの登場によって，眼圧上昇に伴う電気生理学的な研究や神経保護薬の開発，豊富な網膜の材料を使った遺伝子解析なども可能になった．眼圧が25～45 mmHgに上昇するRCS (Royal College of Surgeons) ラットも発見されており，網膜神経節細胞死や視神経乳頭陥凹などが観察されている．しかし残念ながらRCSラットにはチロシンキナーゼ遺伝子に変異があり，視細胞の変性が起こることから，緑内障モデルとしては敬遠されている．

次回は，マウスモデルとその他の動物モデルについて述べる．

文　献

1) Ritch R, Shields MB, Krupin T : Animal models of glaucoma. The Glaucomas (2nd ed), p55-69, Mosby-Year Book, St Louis, 1996
2) Gaasterland D, Kupfer C : Experimental glaucoma in the rhesus monkey. *Invest Ophthalmol Vis Sci* **13** : 455-457, 1974
3) Quigley HA, Hohman RM : Laser energy levels for trabecular meshwork damage in the primate eye. *Invest Ophthalmol Vis Sci* **24** : 1305-1307, 1983
4) Quigley HA, Addicks EM : Chronic experimental glaucoma in primates. I. Production of elevated intraocular pressure by anterior chamber injection of autologous ghost red blood cells. *Invest Ophthalmol Vis Sci* **19** : 126-136, 1980
5) Weber AJ, Zelenak D : Experimental glaucoma in the primate induced by latex microspheres. *J Neurosci Methods* **111** : 39-48, 2001
6) Kaufman PL, Lütjen-Drecoll E, Hubbard WC et al : Obstruction of aqueous humor outflow by cross-linked polyacrylamide microgels in bovine, monkey, and human eyes. *Ophthalmology* **101** : 1672-1679, 1994
7) Armaly MF : Aqueous outflow facility in monkeys and the effect of topical corticoids. *Invest Ophthalmol* **3** : 534-538, 1964
8) Rasmussen CA, Kaufman PL : Primate glaucoma models. *J Glaucoma* **14** : 311-314, 2005
9) Quigley HA, Nickells RW, Kerrigan LA et al : Retinal ganglion cell death in experimental glaucoma and after axotomy occurs by apoptosis. *Invest Ophthalmol Vis Sci* **36** : 774-786, 1995
10) Miyahara T, Kikuchi T, Akimoto M et al : Gene microarray analysis of experimental glaucomatous retina from cynomologous monkey. *Invest Ophthalmol Vis Sci* **44** : 4347-4356, 2003
11) Moore CG, Milne ST, Morrison JC : Noninvasive measurement of rat intraocular pressure with the Tono-Pen. *Invest Ophthalmol Vis Sci* **34** : 363-369, 1993
12) Morrison JC, Moore CG, Deppmeier LM et al : A rat model of chronic pressure-induced optic nerve damage. *Exp Eye Res* **64** : 85-96, 1997
13) Ueda J, Sawaguchi S, Hanyu T et al : Experimental glaucoma model in the rat induced by laser trabecular photocoagulation after an intracameral injection of India ink. *Jpn J Ophthalmol* **42** : 337-344, 1998
14) Levkovitch-Verbin H, Quigley HA, Martin KR et al : Translimbal laser photocoagulation to the trabecular meshwork as a model of glaucoma in rats. *Invest Ophthalmol Vis Sci* **43** : 402-410, 2002
15) Shareef SR, Garcia-Valenzuela E, Salierno A et al : Chronic ocular hypertension following episcleral venous occlusion in rats [letter]. *Exp Eye Res* **61** : 379-382, 1995
16) Garcia-Valenzuela E, Shareef S, Walsh J et al : Programmed cell death of retinal ganglion cells during experimental glaucoma. *Exp Eye Res* **61** : 33-44, 1995
17) Johnson EC, Morrison JC, Farrell S et al : The effect of chronically elevated intraocular pressure on the rat optic nerve head extracellular matrix. *Exp Eye Res* **62** : 663-674, 1996

☆　☆　☆

86. 緑内障の動物モデル (2)
—マウスモデル，その他—

岩田 岳
独立行政法人国立病院機構東京医療センター
臨床研究センター(感覚器センター)
分子細胞生物学研究部門

緑内障研究において動物モデルの存在はきわめて重要である．前号では霊長類とラットモデルについて紹介したが，今回はヒトにつぐ情報量と最新の遺伝子改変技術が利用できるマウスモデルについて，その眼球サイズが小さいことから生まれる実験のむずかしさを含めて紹介したい．

はじめに

霊長類や齧歯類モデルによってこれまでに緑内障の発症機序に関する貴重な情報が得られている．しかし，ヒトとの比較において，厳密には眼球の構造も異なっており，病気の進行速度も加速化されている場合もある．ここで紹介する各モデル動物で観察される現象はそのままヒトに当てはまるわけではない．しかし一つひとつの動物モデルは緑内障の一面を捉えていると考えられ，これらの情報を総合的に検討することによって，緑内障に関係する共通なメカニズムの発見につながる可能性がある．この点について，単一あるいは複数の遺伝子についてこれを欠損や過剰発現させる技術が確立しているマウスモデルには期待が寄せられている．

●マウスモデル

マウスモデルはラットモデルの影で開発が遅れていたが，近年目覚しいマウスの遺伝子改変技術の進歩によって，目的とするトランスジェニックマウス，ノックアウトマウス，ノックインマウスなどが容易に作製されるようになり，眼球が小型であるという欠点がありながら，モデル動物として利用される機会が増加している．また，マウスは他の哺乳類に比べてデータベースが整備されており，遺伝子，蛋白質，代謝系，行動パターンに至るまで詳細な情報を手に入れることが可能である．

しかしながら，マウスには緑内障モデルとしての欠点も存在する．マウスとヒトでは視神経乳頭周辺の血管構造が異なることや，篩状板が存在しないなどの違いがあり[1]，眼球の取り扱いについても不利な面がある．その一つに眼圧測定のむずかしさがある．これまでにマウス専用の侵襲式や非侵襲式の眼圧測定法が開発されているが，最も信頼性の高い眼圧測定法としては，角膜の厚さや曲率半径などに影響されない侵襲式の方法がある．圧力計に接続したガラス管の針をマウスの前房に差し込み，眼圧を測定する方法である．この方法によって，異なるマウスの系について10～20 mmHgの眼圧差が存在することが明らかになった[2]．非侵襲式の利点は多数のマウスの眼圧を短い時間で測定できることであるが，角膜の性状に影響される．いずれの方法についても安定した結果を得るにはやはり訓練が必要である．

最近の遺伝子解析研究によってミオシリン，チトクローム *P4501B1*，オプチニュリン，*WDR36* が緑内障遺伝子として発見されているが，これらの遺伝子改変マウス

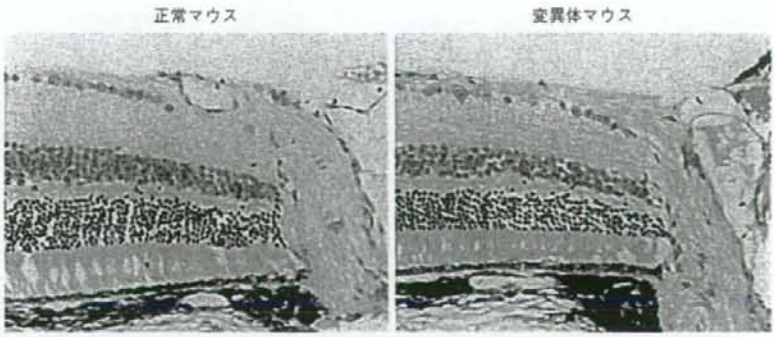

図1 正常マウスとオプチニュリン変異体(Glu50Lys)を発現するトランスジェニックマウスの視神経乳頭
変異体マウスでは網膜神経線維層が菲薄化している．

0910-1810/07/¥100/頁/JCLS

が緑内障を発症するのか研究が行われている．遺伝子改変マウスの利点は発症原因が明確なこと，手術的な方法に比べて表現型が安定していること，そして特別な訓練を必要とせずにネズミ算式に繁殖できることである．すでに複数の緑内障マウスが作製されているが，その一つにミオシリンのTyr437His変異を発現するトランスジェニックマウスがある．このマウスは正常マウスに比べて昼は2 mmHg，夜は4 mmHgの眼圧上昇が認められ，生後1年目には網膜神経節細胞数の20%が減少する[3]．コラーゲンタイプⅠα1サブユニットに遺伝子変異のあるトランスジェニックマウスではコラーゲンのメタロプロテアーゼ（MMP1）による分解が阻害され，生後36週ほどかけて眼圧が4.8 mmHg上昇することが報告されている．隅角の構造は保持されたまま，網膜神経節細胞層への障害が観察され，開放隅角緑内障マウスモデルとして認識されている[4]．また，筆者らはオプチニュリンGlu50Lys変異体を高発現したマウスを作製したところ，正常眼圧は維持されたまま，生後1年後には網膜神経節細胞死や視神経乳頭の陥凹が観察されている．

マウスに対する手術的な眼圧上昇はラットよりもさらに困難である．C57BL/6Jマウスの前房にインドシアニングリーンを注入し，線維柱帯と上強膜静脈部位の光凝固を施すと，約10日後に眼圧が正常なマウスの15.2±0.6 mmHgに対して33.6±1.5 mmHgに上昇したが，60日後には正常値に戻ったと報告されている[5]．網膜神経節細胞層や網膜への機能障害がERG（網膜電図）などによって明らかにされている．Simon Johnらによって報告されたDBA/2Jマウスは2つの遺伝子*Tyrp1*と*Gpnmb*[6]に変異があり，色素顆粒の分散による虹彩の萎縮が起こり，虹彩癒着によって生後9カ月後には眼圧が上昇し，視神経乳頭を基点として網膜神経節細胞死が扇状に観察されている[7]．

●その他の動物モデル

その他の動物モデルにはウサギ，ブタ，ウシなどが報告されているが，広く利用されていない．眼における遺伝子の機能をすばやくおおざっぱに調べる方法として，ゼブラフィッシュ（zebrafish）を利用した研究が最近報告されており，ミオシリン，オプチニュリン，*WDR36*などの欠損による眼球への影響が報告されている[8]．残念ながら眼圧は測定できない．

文　献

1) May CA, Lutjen-Drecoll E : Morphology of the murine optic nerve. *Invest Ophthalmol Vis Sci* **43** : 2206-2212, 2002
2) Savinova OV, Sugiyama F, Martin JE et al : Intraocular pressure in genetically distinct mice : an update and strain survey. *BMC Genet* **2** : 12, 2001
3) Senatorov VV, Malyukova I, Fariss R et al : Expression of mutated mouse myocilin induces open-angle glaucoma in transgenic mice. *J Neurosci* **26** : 11903-11914, 2006
4) Mabuchi F, Lindsey JD, Aihara M et al : Optic nerve damage in mice with a targeted type I collagen mutation. *Invest Ophthalmol Vis Sci* **45** : 1841-1845, 2004
5) Grozdanic SD, Betts DM, Sakaguchi DS et al : Laser-induced mouse model of chronic ocular hypertension. *Invest Ophthalmol Vis Sci* **44** : 4337-4346, 2003
6) Anderson MG, Smith RS, Hawes NL et al : Mutations in genes encoding melanosomal proteins cause pigmentary glaucoma in DBA/2J mice. *Nat Genet* **30** : 81-85, 2002
7) Jakobs TC, Libby RT, Ben Y et al : Retinal ganglion cell degeneration is topological but not cell type specific in DBA/2J mice. *J Cell Biol* **171** : 313-325, 2005
8) McMahon C, Semina EV, Link BA : Using zebrafish to study the complex genetics of glaucoma. *Comp Biochem Physiol C Toxicol Pharmacol* **138** : 343-350, 2004

☆　☆　☆

総説

網膜・硝子体のプロテオーム解析

岩田　岳

〔要　約〕

これまで「遺伝子」「DNA」という言葉をよく見聞きするようになったが，このDNA転写物であるRNAから生成される蛋白質（プロテオーム）の解析が，近年分析技術の向上とともに進歩をみせている。プロテオームはDNAとは異なり，加齢や疾患などの生体の状態によって変化するために，疾患の病態を解明するためだけではなく，体内の微量なプロテオームの変化が疾患の検査・早期診断に応用される可能性が期待されている。プロテオーム解析による網膜硝子体研究への応用と課題について紹介したい。

はじめに

ヒトゲノムプロジェクトが終了し，約2万3千個の遺伝子が発見された。この遺伝子から転写されるRNA（トランスクリプトーム）から10万種類以上のタンパク質が生成されると推察されている（図1）。近年，タンパク質のイオン化技術や質量分析計の精度が向上し，さらにそれを制御・解析ソフトウエアの改良によって，質量分析計の専門技術者でなくても細胞，組織，体液などのタンパク質（プロテオーム）を網羅的に測定し，データを解析することがある程度可能になってきた。健常と病気のプロテオームを比較し，その違いを明らかにすることは，疾患の発症機序を解明するために必要な情報をもたらすだけでなく，疾患バイオマーカーとして早期診断法への応用が期待される。硝子体プロテオームは疾患網膜の状態を反映してダイナミックに変化していると考えられる。網膜疾患によっては脈絡膜毛細血管から網膜成分が漏出し，血漿成分の変化として捉えられる可能性がある。本編ではここ数年間の質量分析計を用いた網膜・硝子体の網羅的タンパク質解析に焦点を絞り，その利用方法と臨床応用への可能性について紹介したい。

Ⅰ．硝子体のプロテオーム

硝子体は眼球内で最も体積を占める透明なゼリー状の組織であり，網膜と接しているために網膜疾患によってその組成は大きく変化していると考え

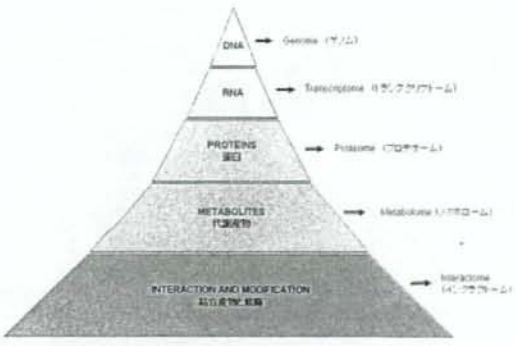

図1　生命現象の研究を総称してフェノミックスという

岩田　岳：独立行政法人国立病院機構東京医療センター臨床研究センター（感覚器センター）

られる。硝子体，房水，血漿の蛋白量をそろえて1次元電気泳動を行うと見分けがつかないほど泳動パターンは類似している。これは房水も硝子体も血漿由来の体液であり，血漿を構成する蛋白が硝子体や房水にも多く含まれていることを意味している。これまで我々が扱った房水や硝子体検体の蛋白濃度は出血の有無などによって0.1-1.0 mg/mlであるのに対し，血漿は50-70 mg/mlと50倍以上の蛋白濃度が測定されている。高蛋白濃度の血漿はプロテオミクス（プロテオーム研究）の分野で最も解析が先行しており，1万種類のタンパク質がすでに同定されている。血漿は22種類の蛋白が99%を占めており，微量蛋白は残り1%に含まれている（図2）。質量分析計の性質上，高い濃度で存在する蛋白から検出されるので，血漿を無分画のまま測定するとアルブミン，免疫グロブリン，トランスフェリンなどが検出され，微量タンパク質は検出されにくい。この数年間に22種類の蛋白を除去するための前処理技術として，各タンパク質に特異的な抗体を用いたアフィニティークロマトグラフィーカラムなどが開発されているが，我々は東レ株式会社が開発中の中空繊維（ホロファイバー）を用いた低分子分画装置を利用して，低分子量領域に絞って，微量成分の分画を試みている（図3）。硝子体プロテオームは血漿プロテオームで蓄積されたノウハウを応用して微量タンパク質の同定が今後盛んに行われると予想される。

日本は硝子体プロテオームでこれまで世界をリードしており，これまでに報告された4つのパイオニア的な硝子体プロテオーム研究をご紹介したい。2002年，中西等は糖尿病網膜症（3検体）と黄斑円孔（2検体）の患者の硝子体についてそれぞれ2次元電気泳動，質量分析計を用いて分析した結果，50種類の蛋白を同定し，この内の30は血漿には含まれていないことを明らかにした。IgG，α-antitrypsin，α-2-HS glycoprotein，complement C4断片が糖尿病の硝子体で増加していることを報告している[1]。2003年小山等は糖尿病網膜症患者の硝子体を1次元電気泳動後，質量分析計で分析した結果，84種類の蛋白の同定に成功し，前年に行った2次元電気泳動と合わせて121種類のタンパク質の同定に成功している。4種類の血管促進因子と3種類の抑制因子，PEDF，endostatin，thrombospondinが検出されている[2]。また同年，山根等は黄斑円孔（26検体）の硝子体を2次元電気泳動で分画し，400スポットを確認，78を同定している。同定されたペプチドは18の蛋白に由来しており，この中にはPEDF，prostaglanding-D2 synthase，IRBPが含まれていた。増殖性糖尿病網膜症（33検体）も同様に解析した結果，600スポットを確認し，121を同定した結果，38の蛋白が同定された。EnolaseとCatalaseが糖尿病の硝子体で顕著に増加しており，黄斑円孔の硝子体や糖尿病の血清中には検出されなかった[3]。2005年には大内等が，

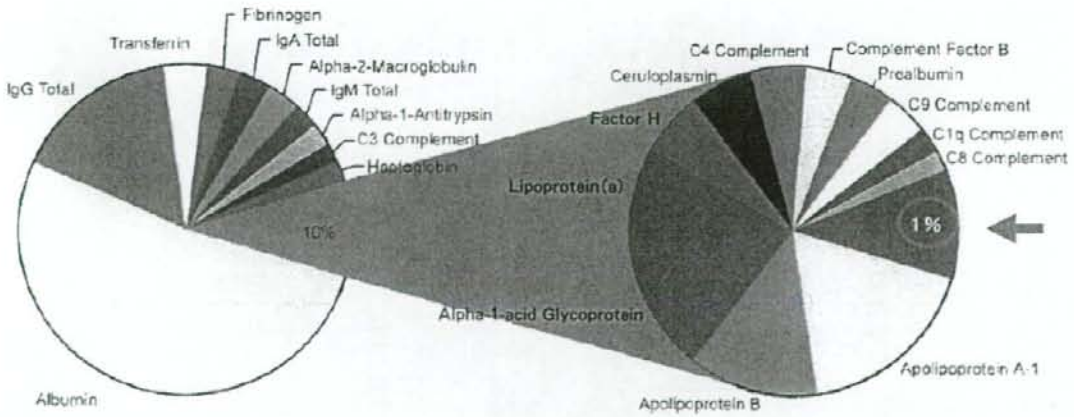

図2　血漿に含まれる蛋白とその割合。22種類のタンパク質が99%を占める

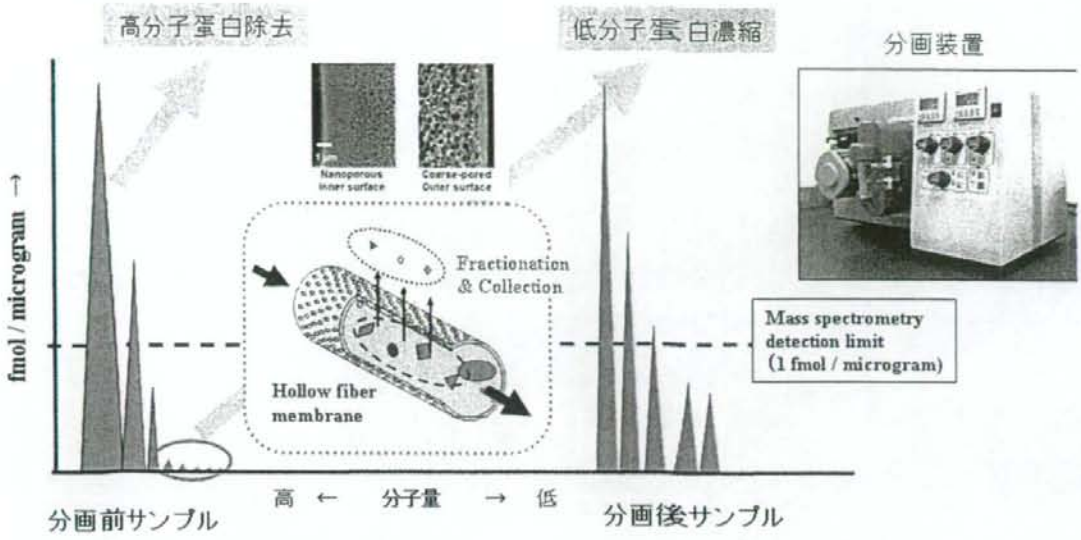

図3 中空紙を使った蛋白分画装置（東レ株式会社製造）による低分子量蛋白の濃縮

増殖性糖尿病初期（Pre-proliferative）で黄斑浮腫（DME）の有無（16：4検体）の硝子体を2次元電気泳動で分画，質量分析計した結果，DMEのグループから14種類の蛋白，non-DMEのグループから15種類の蛋白を同定した。特に8スポットは顕著にDMEグループで増加しており，そのうちの6つのスポットはPEDF, ApoA-4, Trip-11, RPBP, VDBPと同定された[4]。

硝子体サンプルは手術中に破棄されるものを倫理委員会の承認と文書による本人の了解を得て集められているが，検体の多くは病態末期のものが多く，これらの検体を解析しても疾患初期の硝子体の様子を知ることができない。また，日本では健常者眼球の硝子体を集めることができないために，ベースとなるデータが不足している。

Ⅱ．網膜疾患を早期発見するための血漿バイオマーカーの探索

近年，全ゲノム配列が解読された結果，ゲノム上には平均で1,000塩基に1つの割合で異なる配列が存在することが明らかになった。この遺伝子多型(SNP：Single Nucleotide Polymorphism)の生理作用への影響についてはまだ明らかにされていないが，その利用方法については注目されている。ゲノム上の1つのSNPあるいは隣接する複数のSNPを組み合わせてブロックにし，これらと疾患の関連を調べる。同染色体に位置するSNPの組み合わせをハプロタイプと呼ぶが，全てのハプロタイプを明らかにするために国際ハップマッププロジェクト（http://www.hapmap.org/）が進行中である。3×10^9塩基から構成されるゲノム上には1千万個のSNPが存在すると計算されるが，これだけのSNP数を安価に効率よく解析することは技術的に困難であった。しかし，最近，シリコンベースのDNAチップによって数十万個のSNPを同時に検出することができるようになってきた。この方法によって，すでに加齢黄斑変性の2つのリスク遺伝子（*CFH, Htra 1*）が同定されており，発症前にリスクの高い人を選別することが可能になってきた。しかし遺伝子情報だけでは発症の時期まで予測することは困難であり，発症前の蛋白の量的・質的変化を捉えて発症を予測する方法が検討されている。発症前に健常者の硝子体を検査目的で採取することはきわめて困難であり，これを血漿や尿で代行できるかが課題となっている。網膜・脈絡膜から漏れた蛋白が全身への循環によって希釈されることになり，この微量な変化を検出する精度が求められる。

我々は東京医科大学の西村俊秀客員教授との共

同研究によって血漿蛋白の微量変化を質量分析計によって検出できるか研究している。年齢65～88歳の加齢黄斑変性患者6名と白内障患者6名の血液を採血後3分以内に遠心分離によって得た血漿を用いている。血漿からアルブミンと免疫グロブリンを分離して，これを1次元電気泳動でさらに分画しても2疾患の泳動パターンに差は観察されないが，質量分析のマスクロマトグラムとマススペクトルを擬似的な2次表示にすると微量蛋白の変化が観察されるようになった。我々は同様な研究によって，発症前後の血漿サンプルによって疾患バイオマーカーの存在を検証したいと考えている。

Ⅲ．質量分析計を用いたドルーゼンのプロテオーム

最近の研究によって加齢黄斑変性に関係が深いとされてきたドルーゼンの構成蛋白が明らかになり，疾患と補体との関係が注目されている。HagemanやAnderson等は糸球体腎炎の患者で眼底にドルーゼンが観察されることから，糸球体の炎症に関わる補体の活性化が網膜下でも起こっていると推測し，免疫染色法によってこれを証明した[5,6,7]。さらに，Hollyfield等もドルーゼンを抽出して，質量分析計によって蛋白組成を解析した結果，補体活性分子の存在を確認した[8]。ドルーゼン内で発見された蛋白にはアミロイドβや酸化ストレス関連分子など，補体活性化の原因になりうる蛋白が確認されている。

ヒトと同様に黄斑が発達している霊長類において，1970年代から加齢黄斑変性モデルの探索が行われてきた。独立行政法人医薬基盤研究所霊長類医科学研究センターにおいて生後2年でドルーゼンを発症するカニクイザルが社団法人予防衛生協会の鈴木通弘等によって発見され[9]，1頭の疾患個体から交配実験によって大家系に繁殖することに成功した（図4）。我々は厚生労働科学研究難治性疾患克服研究事業として研究班を組織して，ヒトと同様な方法によって疾患個体のドルーゼンを抽出し，プロテオーム解析と免疫染色法によって蛋白組成を解析した。その結果，補体活性分子，抑制分子，クリスタリンなど，ヒトに類似する蛋白組成が含まれることが明らかになった。疾患サルはヒトが50年以上かけて蓄積するドルーゼンと同成分のドルーゼンをわずか2年で生成していることになる。疾患は家系内で優性遺伝することから，単一遺伝子の変異によって発症していると考えられ，この原因遺伝子の同定はドルーゼン生成のメカニズムに関わる重要な情報をもたらすと期待している。

Ⅳ．黄斑のプロテオーム

霊長類と一部の鳥類などで発達している黄斑は視力を決定する重要な部位である。黄斑は錐体細胞が高密度に存在し，周辺網膜に比べて特徴ある構造をしていることから黄斑と周辺網膜との差を分子レベルで解明するために，転写産物（トランスクリプトーム）の解析が行われ，黄斑特異的な遺伝子発現も報告されている。この研究の延長線上には黄斑のプロテオーム解析が考えられるが，今日まで報告されていない。その理由には1）一般的な実験動物であるマウスやラットには黄斑が存在しないこと，2）黄斑部組織が微量であること，3）新鮮な黄斑を多数に手に入れることが困難であることなどが考えられる。我々は霊長類医科学研究センターにおいて研究目的に安楽死された13～19歳の正常なオスザル8頭から黄斑部と網膜周辺部を3 mm径の円柱でくり抜き，これを16眼球について採取し，黄斑と周辺網膜の蛋白抽出液を準備した。これを2次元電気泳動によって分画し，黄斑と周辺網膜の泳動パターンから，それぞれに特異的なスポットを複数発見した。これらのスポットをゲルからくり抜き，ペプチドに分解した後に，質量分析計した結果，これまで発見されなかった複数のタンパク質が同定されてきた。黄斑疾患とこれらのタンパク質との関係については研究が続けられている。

Ⅴ．網膜・硝子体プロテオーム解析の今後の課題

日進月歩の質量分析計の技術革新はこれまで不可能であった蛋白の網羅的解析を可能にし，電気泳動で分画されたスポットを容易に同定できるようになった。眼科分野でもヒトの硝子体，房水，

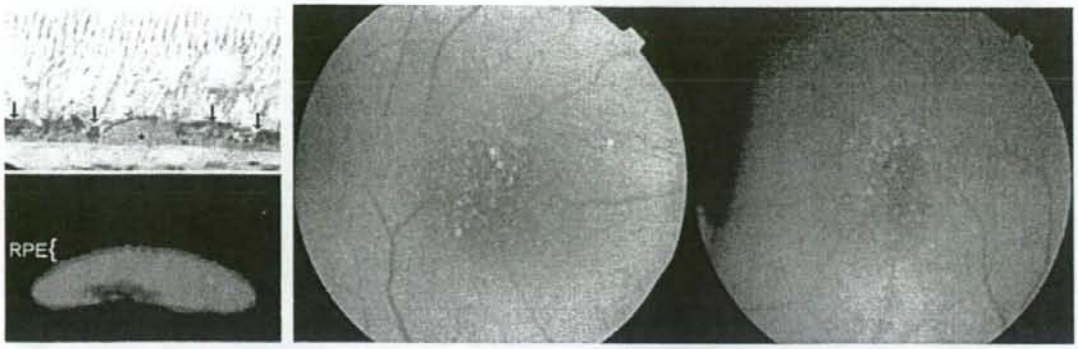

図4 独立行政法人医薬基盤研究所霊長類医科学研究センターで発見された若年性黄斑変性カニクイザルの眼底写真（右）とドルーゼン（左上）およびドルーゼン中の補体活性化（左下）

涙液の網羅的プロテオーム解析，トランスジェニックやノックアウトマウスの眼組織のプロテオーム解析などが行われている。また，最新機器と解析ソフトを利用するとリン酸化，糖，脂質の修飾を受けた蛋白の同定や修飾されたアミノ酸の特定も可能になった。我々は黄斑に特異的な蛋白を探索する過程で，リン酸化蛋白の量的変化を観察している。蛋白修飾の生理的な意味や疾患との関係は今後明らかにされていくと期待される。このような網羅的修飾蛋白の解析はプロテオミクスによって初めて可能になった技術である。

質量分析計にも克服されなければならない弱点が存在する。その一つに質量分析計には定量性が欠けることである。サンプル間に含まれる特定の蛋白について量的変化を高い精度で測定することができない。これまでは電気泳動後のバンドやスポットの濃さとして測定されたり，比較するサンプルを異なる同位体元素でそれぞれラベルして，質量分析計によってラベル化されたペプチドの検出回数として測定されたりする方法が行われてきた。同定した蛋白の定量性について今後の技術開発が望まれている。

おわりに

これまで利用されてきたDNAチップを使った網羅的なトランスクリプトーム解析に加え，これにプロテオーム解析を組み合わせることによって，解析する領域を遺伝子発現から蛋白発現までに広げることが可能になった。DNAチップによって23,000遺伝子の変化を観察し，同時に蛋白の有無を観察することができる。我々も同様な方法によって網膜色素上皮細胞を特異的に増殖させる因子（REF-1/TFPI-2）の作用機序を研究している[10]。この研究では発現量が変化する蛋白間の関係を裏付けるデータとして，遺伝子発現データを利用した。今後はここへ蛋白修飾のデータも加わり，フェノミックスの世界へ一歩近づき，疾患の理解，診断法の開発，さらには治療へと発展するものと期待される。

［文　献］

1) Nakanishi T, et al: Catalogue of soluble proteins in the human vitreous humor: comparison between diabetic retinopathy and macular hole. J Chromatogr B Analyt Technol Biomed Life Sci 776：89-100, 2002.
2) Koyama R, et al: Catalogue of soluble proteins in human vitreous humor by one-dimensional sodium dodecyl sulfate-polyacrylamide gel electrophoresis and electrospray ionization mass spectrometry including seven angiogenesis-regulating factors. J Chromatogr B Analyt Technol Biomed Life Sci 792：5-21, 2003.
3) Yamane K, et al: Proteome analysis of human vitreous proteins. Mol Cell Proteomics 2：1177-1187, 2003.
4) Ouchi M, et al: Proteomic analysis of vitreous from diabetic macular edema. Exp Eye Res 81：176-182, 2005.
5) Hageman GS, et al: Vitronectin is a constituent of ocular drusen and the vitronectin gene is expressed in human retinal pigmented epithelial cells. FASEB J 13：477-484, 1999.

6) Mullins RF, et al: Drusen associated with aging and age-related macular degeneration contain proteins common to extracellular deposits associated with atherosclerosis, elastosis, amyloidosis, and dense deposit disease. FASEB J 14：835-846, 2000.
7) Crabb JW, et al: Drusen proteome analysis: an approach to the etiology of age-related macular degeneration. Proc Natl Acad Sci U S A 99：14682-14687, 2002.
8) Umeda S, et al: Early-onset macular degeneration with drusen in a cynomolgus monkey (Macaca fascicularis) pedigree: exclusion of 13 candidate genes and loci. Invest Ophthalmol Vis Sci 46：683-691, 2005.
9) Umeda S, et al: Molecular composition of drusen and possible involvement of anti-retinal autoimmunity in two different forms of macular degeneration in cynomolgus monkey (Macaca fascicularis). FASEB J 19：1683-1685, 2005.
10) Shibuya M, et al: Proteomic & Transcriptomic Analyses of Retinal Pigment Epithelial Cells Exposed to REF-1/TFPI-2, a Growth Promoting Factor. Invest Ophthal Vis Sci 48：516-521, 2007.

Proteomic and Transcriptomic Analyses of Retinal Pigment Epithelial Cells Exposed to REF-1/TFPI-2

Masahiko Shibuya,[1,2] Haru Okamoto,[1] Takehiro Nozawa,[3] Jun Utsumi,[4] Venkat N. Reddy,[5] Hirotoshi Echizen,[2] Yasuhiko Tanaka,[6] and Takeshi Iwata[1]

Purpose. The authors previously reported a growth-promoting factor, REF-1/TFPI-2, that is specific to retinal pigment epithelial (RPE) cells. The purpose of this study was to determine the genes and proteins of human RPE cells that are altered by exposure to TFPI-2.

Methods. Human primary RPE cells were cultured with or without TFPI-2. Cell extracts and isolated RNA were subjected to proteomic and transcriptomic analyses, respectively. Proteins were separated by two-dimensional gel electrophoresis followed by gel staining and ion spray tandem mass spectrometry analyses. Transcriptomic analysis was performed using a DNA microarray to detect 27,868 gene expressions.

Results. Proteomic analysis revealed c-Myc binding proteins and ribosomal proteins L11 preferentially induced by TFPI-2 in human RPE cells. Transcriptomic analysis detected 10,773 of 33,096 probes in the TFPI-2 treated samples, whereas only 2186 probes were detected in the nontreated samples. Among the genes up-regulated by TFPI-2 at the protein level were c-*myc*, Mdm2, transcription factor E2F3, retinoblastoma binding protein, and the *p21* gene, which is associated with the c-*myc* binding protein and ribosomal protein L11.

Conclusions. The mechanisms by which TFPI-2 promotes the proliferation of RPE cells may be associated with augmented c-*myc* synthesis and the activation of E2F in the retinoblastoma protein (Rb)/E2F pathway at the G1 phase of the RPE cells. Activation of ribosomal protein L11 and the Mdm2 complex of the p53 pathway may be counterbalanced by the hyperproliferative conditions. (*Invest Ophthalmol Vis Sci.* 2007;48: 516–521) DOI:10.1167/iovs.06-0434

Retinal pigment epithelial (RPE) cells play important roles in maintaining the homeostasis of the retina. RPE cells, located between the sensory retina and the choroidal blood supply, form a diffusion barrier controlling access to the subretinal space, with the RPE membrane regulating the transport of proteins and controlling the hydration and ionic composition of the subretinal space. The sensitivity and viability of the photoreceptors thus depend on RPE-catalyzed transport activity. Proteins in the RPE cells that function in ionic, sugar, peptide, and water transport have been identified.[1] Damage to RPE cells generally leads to degeneration of the neural retina, as occurs in retinitis pigmentosa and age-related macular degeneration. Transplantation of the healthy retinal pigment cells or embryonic stem cells differentiating into RPE cells would be an ideal therapeutic approach to treat such diseases, and such attempts have been made.[2]

An alternative approach to treat these retinal diseases would be the use of a growth factor that promotes proliferation of the remaining RPE cells in a damaged retina or one that stimulates the regeneration of damaged RPE cells. To find such factor(s), the proteins expressed in human fibroblast cells were fractionated and assayed, leading to the isolation of RPE cell factor-1 (REF-1), which selectively promoted the proliferation of primary human RPE cells.[3]

Subsequently, the cDNA of REF-1 was cloned using information from the N-terminal amino acid sequences, which was identical with the tissue factor pathway inhibitor-2 (TFPI-2).[3] Earlier studies have shown that TFPI-2 is a Kunitz-type serine protease inhibitor[4–6] involved in the regulation of extrinsic blood coagulation[4,7] and in the proliferation, invasion, and metastasis of various types of malignant cells.[4,8–13] Extensive studies on the physiological roles of TEPI-2 have revealed that the ERK/MAPK pathway[13] may be associated with the up-regulation of the *TFPI-2* gene and that DNA methylation[9,10] in certain tumor cell lines may be related to the downregulation of the *TEPI-2* gene. When TFPI-2 is added to the culture medium of vascular smooth muscle cells, it promotes cell proliferation.[14]

Our initial finding that TFPI-2 enhanced RPE proliferation prompted us to question how this was achieved. We applied proteomic and transcriptomic analyses to screen the changes in the expression of the RNAs and proteins in RPE cells and will show that the proliferation promoting activity of TFPI-2 on RPE cells is associated with the regulation of an oncogene product, c-*myc*, and representative cancer repressor proteins retinoblastoma protein (Rb)/E2F and p53.

Materials and Methods

TFPI-2 Treatment of Human RPE Cell Culture

Human primary RPE cells (passage 5) were seeded at a density of 2.5×10^4 cells/0.5 mL per well in 24-well plastic plates (BD Biosciences, Franklin Lakes, NJ) with Dulbecco modified MEM (DMEM; Invitrogen Japan, Tokyo, Japan) containing 15% fetal calf serum (FCS, Invitrogen). TFPI-2 was added to 20 wells with the RPE cells at 10 ng/mL concentrations and was incubated at 37°C for 24 hours for the proteomic samples, and for 6 hours, 12 hours, and 24 hours for the transcriptomic samples. An equal amount of saline was added to 20 wells containing RPE cells for controls. TFPI-2 was donated by Toray Industries, Inc., Tokyo, Japan.

From the [1]Laboratory of Cellular and Molecular Biology, National Institute of Sensory Organs, National Hospital Organization Tokyo Medical Center, Tokyo, Japan; [2]Department of Pharmacotherapy, Meiji Pharmaceutical University, Tokyo, Japan; [3]Analytical Instrument Division, AMR Inc., Tokyo, Japan; [4]R&D Division, Toray Industries, Inc., Tokyo, Japan; [5]Department of Ophthalmology, Kellogg Eye Center, University of Michigan, Ann Arbor, Michigan; and [6]International University of Health and Welfare, Mita Hospital, Tokyo, Japan.

Supported in part by a grant-in-aid from the policy-based Medical Services Foundation.

Submitted for publication April 18, 2006; revised July 17, 2006; accepted December 4, 2006.

Disclosure: **M. Shibuya**, None; **H. Okamoto**, None; **T. Nozawa**, AMR Inc. (F); **J. Utsumi**, Toray Industries, Inc. (F); **V.N. Reddy**, None; **H. Echizen**, None; **Y. Tanaka**, None; **T. Iwata**, None

The publication costs of this article were defrayed in part by page charge payment. This article must therefore be marked "*advertisement*" in accordance with 18 U.S.C. §1734 solely to indicate this fact.

Corresponding author: Takeshi Iwata, Laboratory of Cellular and Molecular Biology, National Institute of Sensory Organs, National Hospital Organization Tokyo Medical Center, 2-5-1 Higashigaoka, Meguro-ku, Tokyo 152-8902, Japan; iwatatakeshi@kankakuki.go.jp.

Investigative Ophthalmology & Visual Science, February 2007, Vol. 48, No. 2

Protein Sample Preparation

To isolate whole cellular protein extracts from cultured RPE cells, the cells were rinsed 3 times with 1× PBS (pH 7.4) and were lysed in a denaturing lysis buffer containing 7 M urea, 2 M thiourea, 4% CHAPS, 40 mM Tris, 0.2% purifier (Bio-Lyte, pH range 3–10; Bio-Rad, Hercules, CA), and 50 mM dithiothreitol (DTT). The collected lysate was then centrifuged at 14,000*g* for 15 minutes at 4°C. Proteins in the supernatant were repeatedly concentrated and precipitated and finally desalinated (Readyprep 2-D Cleanup kit; Bio-Rad). The protein concentration in the RPE samples was determined by a modified Lowry method adapted for use with the lysis buffer.

Two-Dimensional Electrophoresis

Protein samples were separated by a two-dimensional electrophoresis method. A 300-μg protein sample was loaded on immobilized pH gradient (IPG) strips (pH 3–10, 7 cm; pH 4–7, 17 cm; Bio-Rad) by in-gel rehydration at 20°C overnight. For the 7-cm strip, isoelectric focusing (IEF) was used for the first dimension at an initial voltage of 250 V for 15 minutes, increased to 4000 V for 2 hours, and held until 20,000 V/h was reached. For the 17-cm strip, the initial voltage was set at 250 V, as for the 7-cm strip. Then the voltage was increased to 10,000 V for 3 hours and was held until 60,000 V/h was reached. Immediately after IEF, the IPG strips were equilibrated for 20 minutes in buffer containing 6 M urea, 2% SDS, 0.375 M Tris (pH 8.8), and 20% glycerol under a reduced condition with 2% DTT (Bio-Rad), followed by another incubation for 10 minutes in the same buffer under alkylating conditions with 2.5% iodoacetamide (Bio-Rad).[15]

Equilibrated IPG strips were then electophoresed by SDS-PAGE for the second dimension. Images of the chemiluminescent signals were captured and merged with those of protein spots made visible by protein gel stain (Sypro Ruby; Bio-Rad), and the spots corresponding to the immunoreactivity were cut out. To test reproducibility, the experiment was performed twice.

Protein Identification by Mass Spectrometry

Excised gel pieces were rinsed with water and then with acetonitrile and were completely dried for the reduction-alkylation step. They were incubated with 10 mM DTT in 100 mM ammonium bicarbonate for 45 minutes at 56°C, then with 55 mM iodoacetamide in 100 mM ammonium bicarbonate for 30 minutes at room temperature in the dark. The supernatant was removed, and the washing procedure was repeated three times. Finally, the gel pieces were again completely dried before trypsin digestion and were rehydrated in a solution of trypsin (12.5 ng/μL; Promega, Madison, WI) in 50 mM ammonium bicarbonate. The digestion was continued for 16 hours at 37°C, and the extraction step was performed once with 25 mM ammonium bicarbonate, then twice with 5% formic acid, and finally with water. After resuspension in 40 μL solution of aqueous 0.1% trifluoroacetic acid/2% acetonitrile, the samples were analyzed by liquid chromatography coupled to tandem mass spectrometry (LC-MS/MS). For analysis by LC-MS/MS, the tryptic digests were injected by an automatic sampler (HTS-PAL, CTC Analytics, Zwingen, Switzerland) onto a 0.2 × 50-mm capillary reversed-phase column (Magic C18, 3 μm; Michrom BioResources, Inc., Auburn, CA) using an HPLC (Paradigm MS4; Michrom BioResources). Peptides were eluted with a gradient (95% solvent A consisting of 98% H_2O/2% acetonitrile/0.1% formic acid)/5% solvent B (10% H_2O/90% acetonitrile/0.1% formic acid; 0 minute)/35% solvent A/65% solvent B (20 minutes)/5% solvent A/95% solvent B (21 minutes)/5% solvent A/95% solvent B (23 minutes)/95% solvent A/5% solvent B (30 minutes) for 30 minutes at a flow rate of 1.5 μL/min. Peptides were eluted directly into an ion trap mass spectrometer (ESI; Finnigan LTQ; Thermo Electron Corporation, Waltham, MA) capable of data-dependent acquisition. Each full MS scan was followed by an MS/MS scan of the most intense peak in the full MS spectrum with the dynamic exclusion enabled to allow detection of less-abundant peptide ions. Mass spectrometric scan events and HPLC solvent gradients were controlled with the use of a computer program (Paradigm Home; Michrom BioResources).

Total RNA Isolation from RPE Cells

Total RNA was isolated from the cultured RPE cells after 6 hours, 12 hours, and 24 hours with TFPI-2 using a total RNA isolation kit (RNA-Bee-RNA Isolation Reagent; Tel-Test, Friendswood, TX). Total RNA samples were treated with RNase-free DNase (Roche Diagnostics Japan) to minimize genomic DNA contamination.

DNA Microarray Analysis

DNA microarray analysis was performed (AB1700 Chemiluminescent Microarray Analyzer; Applied Biosystems, Foster City, CA). The survey array used (Human Genome Survey Array; Applied Biosystems) contained 33,096 60-mer oligonucleotide probes representing a set of 27,868 individual human genes and more than 1000 control probes. Sequences used for the microarray probe were obtained from curated transcripts (Celera Genomics Human Genome Database), RefSeq transcripts that had been structurally curated from the LocusLink public database, high-quality cDNA sequences from the Mammalian Gene Collection (MGC; http://mgc.nci.nih.gov), and transcripts that were experimentally validated (Applied Biosystems). The 60-mer oligo probes were synthesized using standard phosphoramidite chemistry and solid-phase synthesis and underwent quality control by mass spectrometry. The probes were deposited and covalently bound to a derivatized nylon substrate (2.5 × 3 inches) that was backed by a glass slide by contact spotting with a feature diameter of 180 μm and more than 45 μm between each feature. A 24-mer oligo internal control probe (ICP) was cospotted at every feature with 60-mer gene expression probe on the microarray. Digoxigenin-UTP labeled cRNA was generated and linearly amplified from 1 μg total RNA (Chemiluminescent RT-IVT Labeling Kit, version 2.0; Applied Biosystems) according to the manufacturer's protocol. Array hybridization (two arrays per sample), chemiluminescence detection, image acquisition, and analysis were performed (Chemiluminescence Detection Kit and AB1700 Chemiluminescent Microarray Analyzer; Applied Biosystems) according to the manufacturer's protocol.

Briefly, each microarray was first prehybridized at 55°C for 1 hour in hybridization buffer with blocking reagent. Sixteen micrograms labeled cRNA targets were first fragmented into 100 to 400 bases by incubation with fragmentation buffer at 60°C for 30 minutes, mixed with internal control target (ICT; 24-mer oligo labeled with LIZR fluorescent dye), and hybridized to each prehybrid microarray in 1.5 mL vol at 55°C for 16 hours. After hybridization, the arrays were washed with hybridization wash buffer and chemiluminescence rinse buffer. Enhanced chemiluminescent signals were generated by first incubating the arrays with anti–digoxigenin alkaline phosphatase and enhanced with chemiluminescence enhancing solution and chemiluminescence substrate.

Images were collected from each microarray using the 1700 analyzer equipped with a high-resolution, large-format CCD camera, including 2 "short" chemiluminescent images (5-second exposure length each) and 2 "long" chemiluminescent images (25-second exposure length each) for gene expression analysis, two fluorescent images for feature finding and spot normalization, and two quality control images for spectrum cross-talk correction. Images were quantified, corrected for background and spot, and spatially normalized.

Data Analysis

MS data were identified with the use of a protein search program (BioWorks 3.2; Thermo Electron Corporation, Waltham, MA). For protein database searches, the same program was used to create centroid peak lists from the raw spectra. These peak lists were then submitted for database searching (BioWorks). The identity of the samples was searched from databases (nrNCBI [www.ncbi.nlm.nih.gov]) that extracted proteins and were restructured; search terms included human and *Homo sapiens*. Differentially expressed proteins were further analyzed for related genes and proteins using natural language processing software (Pubgene database; PubGene Inc., Boston, MA) and data mining software of gene expression (OmniViz; OmniViz, Inc., Maynard, MA).

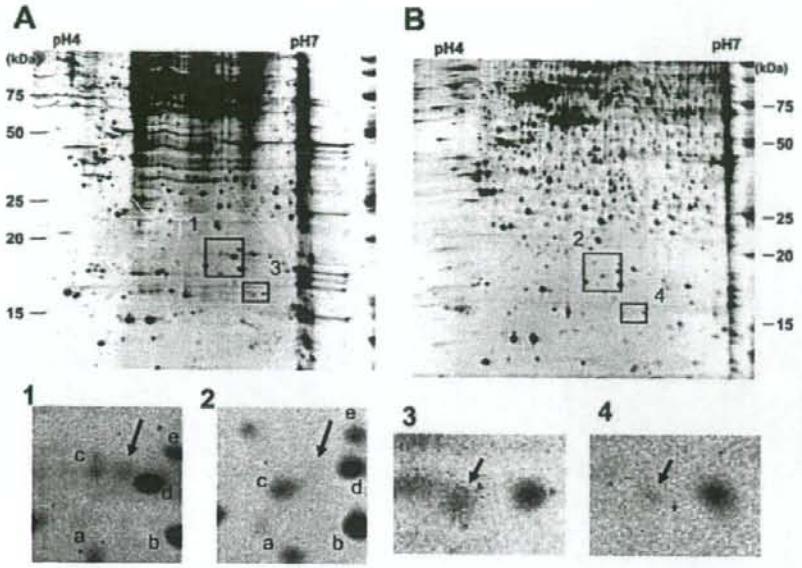

FIGURE 1. Two-dimensional gel electrophoresis of human RPE cells culture with (A) and without (B) TFPI-2. Spots corresponding to proteins whose expression is dependent on the presence of TFPI-2 in the culture medium are indicated by the *arrows* (*insets*). Proteins were detected by SYPRO Ruby staining. Spots corresponding to the differentially expressed proteins indicated by *arrows* (1 vs. 2 and 3 vs. 4) were subsequently subject to the LC-MS/MS analysis so that proteins could be identified.

RESULTS

Proteome Analysis of RPE Cells Treated with TFPI-2

To determine the mechanisms responsible for the proliferation-promoting activity of TFPI-2 on RPE cells, protein synthesis and RNA expression were determined before and after TFPI-2 exposure. Differentially expressed proteins in the primary human RPE cells in response to TFPI-2 were identified by two-dimensional electrophoresis (Fig. 1). Samples were initially separated using IPG at a pH range of 3 to 10 to observe the full distribution of protein spots. The pH range was then narrowed to 4 to 7 to obtain higher resolution for spot picking. Consequently, approximately 480 spots were identified in the whole gel. We then focused on molecular weight less than 25 kDa, which is easy to check for changes. Ten spots considered differentially expressed in the two-dimensional gel were collected and subjected to LC-MS/MS analysis. Among the identified proteins, ribosomal protein L11 (RPL11; Fig. 1-1) and c-Myc binding protein (MYCBP; Fig. 1-3), known for regulating cell proliferation, were identified.[16] These two proteins, identified by LC-MS/MS analysis and data analysis software (Bioworks 3.2), were consistent with those estimated from the results of two-dimensional electrophoresis (Table 1).

Transcriptomic Analysis of RPE Cells Treated with TFPI-2

The expression of 8134 genes in RPE cells was analyzed using DNA microarray with and without TFPI-2 exposure for 6 hours, 12 hours, and 24 hours. Signal normalization was performed for six independent DNA microarray chips according to the manufacturer's protocol. Genes differentially expressed by more than threefold were considered significant and were selected for further analysis. Among the 33,096 possible probes, 10,773 probes were detected in the RPE cells incubated with TFPI-2, whereas only 2186 probes were detected without TFPI-2. Based on expression levels at the three time points (6 hours, 12 hours, and 24 hours), the time-dependent expression pattern of each gene was calculated and clustered with other genes with similar expression patterns using data mining software (OmniViz). Data analysis resulted in 38 clusters of genes that either increased or decreased their expression levels by more than twofold after TFPI-2 (Fig. 2). Nineteen genes were upregulated in 5 clusters, 108 genes in 16 clusters, and 717 genes in 22 clusters at 6 hours, 12 hours, and 24 hours, respectively. For downregulated genes, 30 genes in 16 clusters, 119 genes in 19 clusters, and 3 genes in 19 clusters were observed after 6 hours, 12 hours, and 24 hours, respectively. Transcriptomic analysis revealed significantly more genes differentially expressed at the transcriptional level than at the proteome level.

DISCUSSION

Proteins and genes whose expression was upregulated or downregulated after exposure to TFPI-2 were analyzed in human RPE cells to study the proteomic and transcriptomic changes. Protein and gene expression profiles for human RPE cells have been reported by West et al.,[17] who identified 278 proteins, and Cai et al.,[18] who reported 5580 ± 84 genes expressed in adult human RPE and ARPE19 cell lines using a DNA chip with 12,600 probes (Human U95Av2; Affymetrix, Santa Clara, CA). Our study showed changes in the expression of 8134 of 27,868 genes. DNA microarray analyses were simul-

TABLE 1. Two-Dimensional Gel Spots Identified by Mass Spectrometry

Protein	Number of AA	Peptide Residues	Identified Peptide from Database	MW	Score	Accession Number
c-Myc binding protein	167	108–117	TAEDAKDFFK	18642.6	10.13	1731809
Ribosomal protein L11	177	88–94	VREYELR	20125.1	20.21	14719845

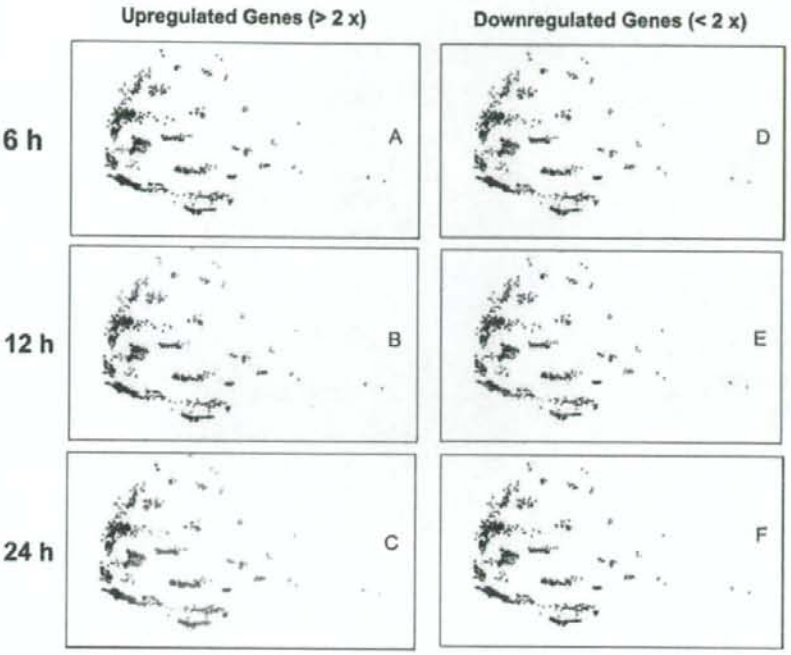

FIGURE 2. Differentially expressed genes detected by DNA array are plotted as clusters. Differentially expressed genes whose expression level was increased by more than twofold (A–C) or was reduced by more than 0.5-fold (D–F) in RPE cells treated with TFPI-2 at incubation times of 6 hours, 12 hours, and 24 hours compared with the control cells are shown. Expression profile analysis revealed different gene expression patterns at each incubation time.

taneously performed at three time points (6 hours, 12 hours, and 24 hours) to monitor the course of expression of the possible 27,868 genes in human RPE cells exposed and not exposed to TFPI-2. This study was conducted at the translational and the transcriptional levels to complement the disadvantages of each method.

Raw gene expression data were further analyzed with data mining software (OmniViz) to obtain an overall picture of the transcriptional changes induced by TFPI-2 in human primary RPE cells. Genes whose expressions were changed by more than twofold were clustered into 38 groups showing a change of expression at each time point (Fig. 2). The number of genes upregulated at each time point was considerably higher than the number that was downregulated. A small number of genes was triggered by TFPI-2 treatment at 6 hours, before the major changes occurred at 24 hours. Among the initially upregulated genes were reticulon 4 interacting protein 1, phospholipase C, delta 1, granzyme M (lymphocyte met-ase 1; *GZMM*), and mitochondrial ribosomal protein L41 (*MRPL41*).

Proteomics analysis simultaneously performed at 24 hours identified two differentially expressed proteins, the c-*myc* binding protein (MYCBP) and the ribosomal protein L11 (RPL11). MYCBP and RPL11 (Fig. 3) are well known to regulate cell cycling through the Rb/E2F pathway and the p53 pathway, respectively. MYCBP stimulates c-*myc* transcription through the retinoblastoma protein (Rb)/E2F pathway (see Fig. 5). Sears et al.[19] reported that activation of Myc increased the signal transduction of the cyclin D/cdk4 and cyclin E/cdk2 pathways. Activation of these pathways inactivates Rb after phosphorylation and E2F dissociation, which then promotes RPE cells to go into the S-phase of the cell cycle. The twofold transcriptional increase of *Rb* and *E2F3* in TFPI-2 exposed cells compared with control at 24 hours supports this hypothesis (Figs. 4C, 4F).

Concomitantly, the expressions of Rb and Mdm2 were upregulated twofold in growth-stimulated cells compared with control cells. Because Rb is associated with the negative regulation of the G_1-phase of the cell cycle, the enhanced expres-

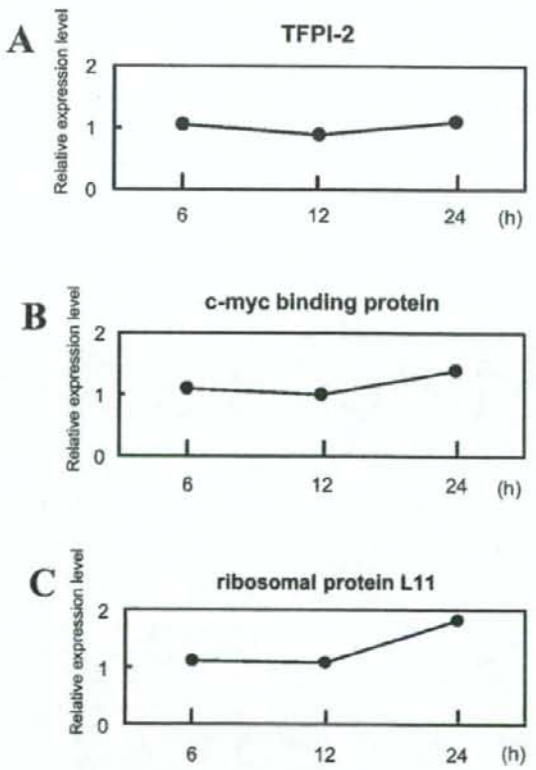

FIGURE 3. Time course of gene expression for TFPI-2 (A), c-*myc* binding protein (B), and ribosomal protein L11 (C) in the cultured human RPE cells after exposure to TFPI-2.

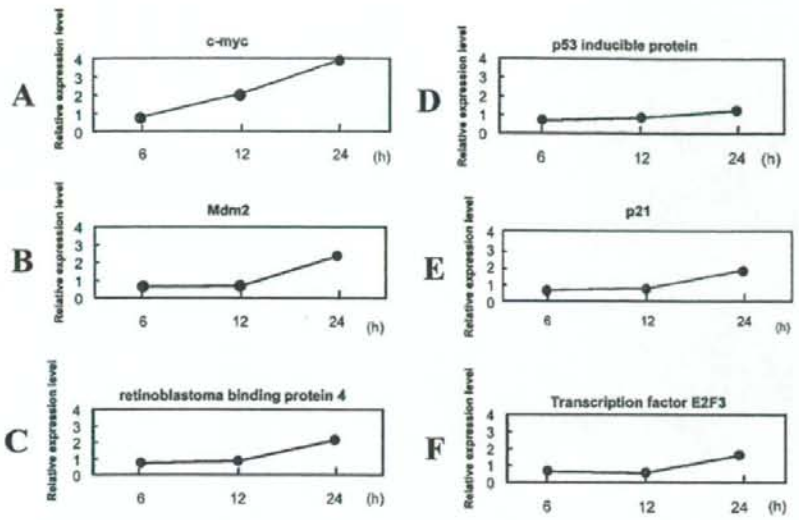

FIGURE 4. Time courses of protein expression patterns for c-*myc* (A), Mdm2 (B), retinoblastoma binding protein 4 (C), p-53 inducible protein (D), p21 (E), and transcription factor E2F3 in the cultured human RPE cells after exposure to TFPI-2.

sion of *Mdm2* might have been involved in the augmented degradation of Rb through the ubiquitin/proteasome-dependent pathway. Recently, Uchida et al.[20] suggested that Mdm2 regulates the function of RB through the ubiquitin-dependent degradation of RB.

The *Rb* gene was the first identified tumor-suppressor gene,[21] and it was recognized as a central component of a signaling pathway that controlled cell proliferation. Specifically, the D-type G_1 cyclins, together with their associated cyclin-dependent kinases (CKDs) Cdk4 and Cdk6, initiated the phosphorylation of Rb and Rb family members, inactivating their capacity to interact with the E2F transcription factors (Fig. 5).[19] This phosphorylation leads to an accumulation of E2F1, E2F2, and E2F3a, which activate the transcription of a large number of genes essential for DNA replication and further cell cycle progression.[22-26] Among the E2F targets are genes encoding a second class of G_1 cyclins, cyclin E, and the associated kinase Cdk2 (Fig. 5).[19] The activation of cyclin E/Cdk2 kinase activity by E2F leads to further phosphorylation and inactivation of Rb, further enhancing E2F activity and increasing the accumulation of cyclin E/Cdk2 (Fig. 5).[19] This feedback loop, which leads to a continual inactivation of *Rb* independent of the action of cyclin D/Cdk4—defined as a junction in cell proliferation response when passaged through the cell cycle—becomes growth factor independent.[25,26] The activity of the G_1 Cdks is negatively regulated by a family of cyclin-dependent kinase inhibitors (CKIs), including $p21^{WAF1}$, $p27^{Kip1}$, and the $p16^{INK4a}$ family.[27] The three upregulated E2Fs associate exclusively with Rb and appear to play a positive role in cell cycle progression.[19]

RPL11 binds the mouse double-minute 2 (Mdm2 is the mouse homologue of Hdm2 in humans) protein with other ribosomal proteins (L23 and L5) to form a complex to inhibit ubiquitin-dependent degradation of p53.[28-30] The RPL11 protein is expressed in ARPE-19 cells.[31] Inhibition of p53 degradation leads to p21 signaling, which participates in the G_1

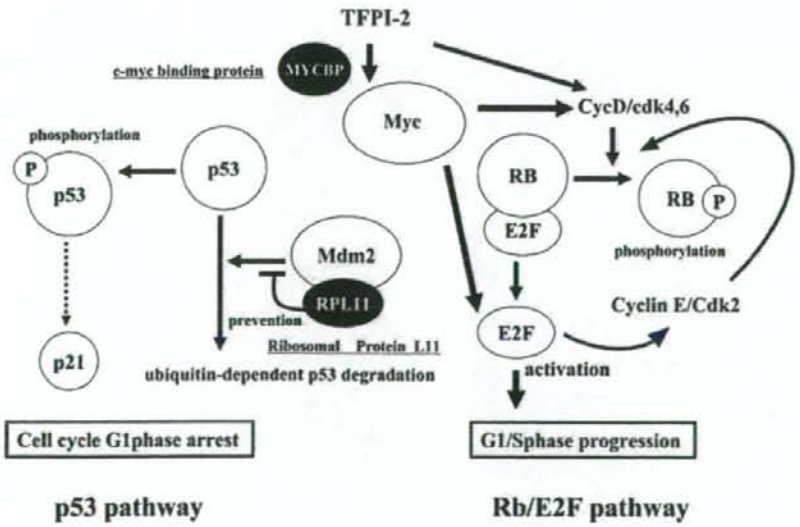

FIGURE 5. Hypothetical network of various genes and proteins associated with the growth-promoting effect of TFPI-2 on the human RPE cells. *Arrows*: stimulatory signals. *Straight* and *dotted lines*: inhibitory effects.

arrest of the cell cycle but also negatively regulates cell proliferation (Fig. 5).[30,32–34] In support of this hypothesis, *p21* transcription was increased by twofold after 24 hours by TFPI-2.

The *p53* gene mediates a major tumor-suppression pathway in mammalian cells and is frequently altered in human tumors.[30] Its function is kept at a low level during normal cell growth and is activated in response to various cellular stresses by acting as a sequence-specific transcription factor.[30] The p53 protein induces cell cycle arrest or apoptosis.[30]

Shinoda et al.[14] reported cell growth proliferation of vascular smooth muscle endothelial cells by a purified mitogenic substance from human umbilical vein endothelial cells, later identified as TFPI-2. These authors showed the rapid activation of mitogen-activated protein kinase (MAPK) by TFPI-2 and the induced activation of proto-oncogene *c-fos* mRNA in smooth muscle cells.[14] They concluded that *c-fos* activation was initiated by MAPK based on MAPK inhibitor PD098059 suppression.

In conclusion, the results of proteomic and transcriptomic analyses suggest that the proliferation of RPE cells induced by TFPI-2 is regulated through the Rb/E2F, p53, and Ras/Raf/MAPK pathways. We and others[4,35] have reported a transcript of TFPI-2 in the mRNA of RPE cells. It is now reasonable to expect that RPE cells are able to self-proliferate by generating TFPI-2. Additional studies are needed to determine whether TFPI-2 can act as such an autocrine factor and can be modified for future treatment of the dry-type age-related macular degeneration and of retinitis pigmentosa.

References

1. Hughes BA, Gallemore RP, Miller SS. Transport mechanisms in the retinal pigment epithelium. In: Marmor MF, Wolfensberger TJ, eds. *The Retinal Pigment Epithelium: Function and Disease*. New York: Oxford University Press; 1998:103–134.
2. Haruta M. Embryonic stem cells: potential source for ocular repair. *Semin Ophthalmol*. 2005;20:17–23.
3. Tanaka Y, Utsumi J, Matsui M, et al. Purification, molecular cloning, and expression of a novel growth-promoting factor for retinal pigment epithelial cells, REF-1/TFPI-2. *Invest Ophthalmol Vis Sci*. 2004;45:245–252.
4. Chand HS, Foster DC, Kisiel W. Structure, function and biology of tissue factor pathway inhibitor-2. *Thromb Haemost*. 2005;94:1122–1130.
5. Schmidt AE, Chand HS, Cascio D, et al. Crystal structure of Kunitz domain 1 (KD1) of tissue factor pathway inhibitor-2 in complex with trypsin: implications for KD1 specificity of inhibition. *J Biol Chem*. 2005;280:27832–27838.
6. Chand HS, Schmidt AE, Bajaj SP, et al. Structure-function analysis of the reactive site in the first Kunitz-type domain of human tissue factor pathway inhibitor-2. *J Biol Chem*. 2004;279:17500–17507.
7. Sprecher CA, Kisiel W, Mathewes S, et al. Molecular cloning, expression, and partial characterization of a second human tissue-factor-pathway inhibitor. *Proc Natl Acad Sci USA*. 1994;91:3353–3357.
8. Yanamandra N, Kondraganti S, Gondi CS, et al. Recombinant adeno-associated virus (rAAV) expressing TFPI-2 inhibits invasion, angiogenesis and tumor growth in a human glioblastoma cell line. *Int J Cancer*. 2005;115:998–1005.
9. Rollin J, Iochmann S, Blechet C, et al. Expression and methylation status of tissue factor pathway inhibitor-2 gene in non-small-cell lung cancer. *Br J Cancer*. 2005;92:775–783.
10. Konduri SD, Srivenugopal KS, Yanamandra N. Promoter methylation and silencing of the tissue factor pathway inhibitor-2 (TFPI-2), a gene encoding an inhibitor of matrix metalloproteinases in human glioma cells. *Oncogene*. 2003;22:4509–4516.
11. Santin AD, Zhan F, Bignotti E, et al. Gene expression profiles of primary HPV16- and HPV18-infected early stage cervical cancers and normal cervical epithelium: identification of novel candidate molecular markers for cervical cancer diagnosis and therapy. *Virology*. 2005;331:269–291.
12. Sato N, Parker AR, Fukushima N, et al. Epigenetic inactivation of TFPI-2 as a common mechanism associated with growth and invasion of pancreatic ductal adenocarcinoma. *Oncogene*. 2005;24:850–858.
13. Kast C, Wang M, Whiteway M. The ERK/MAPK pathway regulates the activity of the human tissue factor pathway inhibitor-2 promoter. *J Biol Chem*. 2003;278:6787–6794.
14. Shinoda E, Yui Y, Hattori R, et al. Tissue factor pathway inhibitor-2 is a novel mitogen for vascular smooth muscle cells. *J Biol Chem*. 1999;274:5379–5384.
15. Bahk SC, Lee SH, Jang JU, et al. Identification of crystallin family proteins in vitreous body in rat endotoxin-induced uveitis: involvement of crystallin truncation in uveitis pathogenesis. *Proteomics*. 2006;6:3436–3444.
16. Taira T, Maëda J, Onishi T, et al. AMY-1, a novel C-MYC binding protein that stimulates transcription activity of C-MYC. *Genes Cells*. 1998;3:549–565.
17. West KA, Yan L, Shadrach K, et al. Protein database, human retinal pigment epithelium. *Mol Cell Proteomics*. 2003;2:37–49.
18. Cai H, Del Priore LV. Gene expression profile of cultured adult compared to immortalized human RPE. *Mol Vis*. 2006;12:1–14.
19. Sears RC, Nevins JR. Signaling networks that link cell proliferation and cell fate. *J Biol Chem*. 2002;277:11617–11620.
20. Uchida C, Miwa S, Kitagawa K, et al. Enhanced Mdm2 activity inhibits pRB function via ubiquitin-dependent degradation. *EMBO J*. 2005;24:160–169.
21. Hanahan D, Weinberg RA. The hallmarks of cancer. *Cell*. 2000;100:57–70.
22. Dyson N. The regulation of E2F by pRB-family proteins. *Genes Dev*. 1998;12:2245–2262.
23. Nevins JR. Toward an understanding of the functional complexity of the E2F and retinoblastoma families. *Cell Growth Differ*. 1998;9:585–593.
24. Harbour JW, Dean DC. Rb function in cell-cycle regulation and apoptosis. *Nat Cell Biol*. 2000;2:E65–E67.
25. Dou QP, Levin AH, Zhao S, Pardee AB. Cyclin E and cyclin A as candidates for the restriction point protein. *Cancer Res*. 1993;53:1493–1497.
26. Pardee AB. A restriction point for control of normal animal cell proliferation. *Proc Natl Acad Sci USA*. 1974;71:1286–1290.
27. Sherr CJ, Roberts JM. CDK inhibitors: positive and negative regulators of G1-phase progression. *Genes Dev*. 1999;13:1501–1512.
28. Krystof V, McNae IW, Walkinshaw MD. Antiproliferative activity of olomoucine II, a novel 2,6,9-trisubstituted purine cyclin-dependent kinase inhibitor. *Cell Mol Life Sci*. 2005;62:1763–1771.
29. Dai MS, Lu H. Inhibition of MDM2-mediated p53 ubiquitination and degradation by ribosomal protein L5. *J Biol Chem*. 2004;279:44475–44482.
30. Zhang Y, Wolf GW, Bhat K, et al. Ribosomal protein L11 negatively regulates oncoprotein MDM2 and mediates a p53-dependent ribosomal-stress checkpoint pathway. *Mol Cell Biol*. 2003;23:8902–8912.
31. Rao KC, Palamalai V, Dunlevy JR, et al. Peptidyl-Lys metalloendopeptidase-catalyzed ^{18}O labeling for comparative proteomics: application to cytokine/lipolysaccharide-treated human retinal pigment epithelium cell line. *Mol Cell Proteomics*. 2005;4:1550–1557.
32. Chao C, Saito S, Kang J. p53 transcriptional activity is essential for p53-dependent apoptosis following DNA damage. *EMBO J*. 2000;19:4967–4975.
33. Bai F, Matsui T, Ohtani-Fujita N, et al. Promoter activation and following induction of the p21/WAF1 gene by flavone is involved in G1 phase arrest in A549 lung adenocarcinoma cells. *FEBS Lett*. 1998;437:61–64.
34. Nyunoya T, Powers LS, Yarovinsky TO. Hyperoxia induces macrophage cell cycle arrest by adhesion-dependent induction of p21Cip1 and activation of the retinoblastoma protein. *J Biol Chem*. 2003;278:36099–360106.
35. Ortego J, Escribano J, Coca-Prados M. Gene expression of protease and protease inhibitors in the human ciliary epithelium and ODM-2 cells. *Exp Eye Res*. 1997;65:289–299.